Journal of Structural Geology 172 (2023) 104891

Contents lists available at ScienceDirect

Journal of Structural Geology

journal homepage: www.elsevier.com/locate/jsg

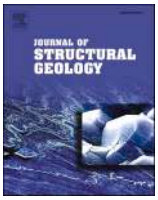

Dyke or pipe? Contributions of magnetic fabrics to the reconstruction of the geometry of an eroded subvolcanic body (Cadí basin, Pyrenees)

Ana Simón-Muzás [a,*], Antonio Casas-Sainz [a], Ruth Soto [b], Elisabet Beamud [c], Josep Gisbert [a]

[a] Departamento de Ciencias de la Tierra, Geotransfer-IUCA, Universidad de Zaragoza, 50009, Zaragoza, Spain
[b] Instituto Geológico y Minero de España (IGME), CSIC, Unidad de Zaragoza, 50006, Zaragoza, Spain
[c] Paleomagnetic Laboratory CCiTUB - Geosciences Barcelona (Geo3Bcn), CSIC, 08028, Barcelona, Spain

ARTICLE INFO

Keywords:
Magnetic fabrics
Intrusive body
Pyrenees

ABSTRACT

The reconstruction of the geometry of igneous bodies in inverted basins is often a difficult task, because most of their volume can be either below or above the topographic surface. Indirect methods, such as the determination of their internal fabric can give clues to constrain geometrical reconstructions. The Sant Salvador intrusion, located in the Late Carboniferous-Permian Cadí basin (Central-Eastern Pyrenees), is a good example for testing the application of magnetic fabrics to shallow igneous bodies because of (i) its characteristics in terms of crystal composition/orientation, showing a homogeneous petrofabric controlled by plagioclase crystals 0.4 mm in size, (ii) its good, though partial, preservation, (iii) its position in the stratigraphical succession, between volcaniclastic sediments and unconformably overlying red beds, and (iv) the many unknown factors related to the intrusion, including the geometry of the body and its depth and the amount of erosion after intrusion. Furthermore, the Sant Salvador intrusion provides opportunity for checking the correspondence between the petrofabric and the magnetic fabrics when the magnetic carriers of susceptibility (with an average value of $5217{\cdot}10^{-6}$ SI) are mainly ferromagnetic. In this case the main magnetic carriers are magnetite and also hematite, the latter resulting from oxidation processes at the paleosurface. The results of Anisotropy of Magnetic Susceptibility show a bimodality in the K_1 disposition after bedding restitution: vertical in the deeper areas of the intrusion and subhorizontal, E-W, in the uppermost stratigraphic positions with an intermediate necking zone in which transition from vertical to horizontal flow is interpreted to occur. Bands deflecting the mineral foliation at the micro scale have also a tectonic or thermal origin but do not seem to interfere with the magnetic ellipsoid axes. Columnar jointing is interpreted to be parallel to the long axis of the intrusion (and therefore to magma flow, and perpendicular to the paleosurface. All these features indicate that the Sant Salvador intrusion can be interpreted as a subvertical pipe feeding a sill that was eroded before the sedimentation of the overlying red beds.

1. Introduction

The formation and growth of igneous bodies represents a widespread process from deep to shallow crustal conditions (e.g., Gudmundsson, 2012; Menand, 2011; Rivalta et al., 2015). However, the mechanisms controlling magma emplacement and the configuration of different body geometries are still a matter of debate, especially when dealing with intrusions at shallow crustal levels (Horsman et al., 2005). One of the factors playing a major role on this process is the depth of emplacement. At shallow depths, space making mechanisms are the primary controls (e.g. roof lifting, floor depression, stopping, e.g. Petraske et al., 1978; Hutton, 1988; Cruden et al., 2017), that can be inferred from the geometry of the body and the deformation of the host rock. However, in ancient records, the geometry of igneous bodies is not often easy to decipher because faulting, folding or erosion of the igneous and the host rocks can hinder their geometrical features. In these cases, other constraints and techniques are necessary to indirectly obtain an approximation to their shape.

The magmatic fabric of igneous bodies is a good indicator of how magma was emplaced (e.g. Cañón-Tapia, 2004). In the same sense, it can give clues to the geometry of igneous intrusions when the shape of the body cannot be outlined, for being most of it either above or below the topographic surface. Although the relationship between geometry and magmatic fabric is not always straightforward, and other constraints are

* Corresponding author.
E-mail address: anasimon@unizar.es (A. Simón-Muzás).

https://doi.org/10.1016/j.jsg.2023.104891
Received 6 July 2022; Received in revised form 18 May 2023; Accepted 18 May 2023
Available online 25 May 2023

also necessary, there are multiple works that show that there is a relationship between these two elements, both for syn-tectonic and post-tectonic intrusions (see, e.g., Román-Berdiel et al., 1995; Leblanc et al., 1996, Gleizes et al., 1998; Aranguren et al., 2003; Sant'Ovaia et al., 2010; Nédélec and Bouchez, 2015).

The analysis of the anisotropy of magnetic susceptibility (AMS) is a useful and rapid technique to assess the petrofabric of rocks (e.g., Jelinek 1981; Kligfield et al., 1983; Tarling and Hrouda 1993; Borradaile and Henry,1997). Applied to igneous rocks, the analysis of AMS constitutes a powerful tool to characterize(i) the primary magmatic flow, (ii) the location of preferential pathways for magma ascent of plutonic, volcanic and subvolcanic rocks, and/or (iii) the deformation undergone before the complete crystallization of plutonic rocks (e.g. Tarling and Hrouda, 1993; Bouchez, 1997; Bascou et al., 2005; Ort et al., 2015).

The Sant Salvador intrusion in the Central Pyrenees provides an excellent setting for AMS application in order to reconstruct the shape of igneous bodies due to (i) its good, although very limited preservation, in terms of outcropping surface, (ii) its position in the stratigraphic series, (iii) its structural characteristics, cutting across a sedimentary succession, and (iv) the existence of suitable outcrops showing parts of the body that were originally at different depths. In this work, the combination of AMS, structural analysis and petrofabric studies contribute to characterize changes in the petrofabric of the Sant Salvador intrusion that can be related to differences in the magma flow pattern, and, ultimately, to its shape. Likewise, AMS interpretation together with the structural data (used to define the pattern of columnar jointing) provide constraints to estimate the geometry and orientation of the intrusive body. This work offers an example where the analysis of the AMS is used to provide insights in (i) the direction of flow of a shallow intrusive body, and (ii) its geometry, where previous studies based exclusively on facies analysis and cartography did not reach a conclusive outcome.

2. Geological setting

The Sant Salvador intrusion is located in the central part of the Cadí basin where it crops out along a NNW-SSE oriented (Fig. 1), 650 m-long ridge (Serrat dels Esquers). The outcrop is located at an elevation of 1633 m, close to the Sant Salvador hermitage. It stands out in the landscape for its steep walls and the exposed, acute longitudinal crest.

The Cadí basin, located in the central-eastern part of the Pyrenean range, is one of the Late Carboniferous-Permian basins of the Iberian Peninsula. It is situated in the southern edge of the Axial Zone and limited between the paracomformable Mesozoic units to the South and the unconformity over the Variscan basement to the South. Its formation has been interpreted as linked to an asymmetric graben (Saura and Teixell, 2006) filled with a variety of volcanic products (Simón-Muzás et al., 2022). At present, rocks cropping out in the Cadí basin (Fig. 1) are integrated in a south-dipping monocline interpreted as the southern limb of a basin-scale hangingwall anticline associated with the Alpine Orri thrust (Muñoz, 1992; Saura and Teixell, 2006).

The Late Carboniferous-Permian rocks of the Cadí basin are subdivided into four lithostratigraphic units according to Gisbert (1981).

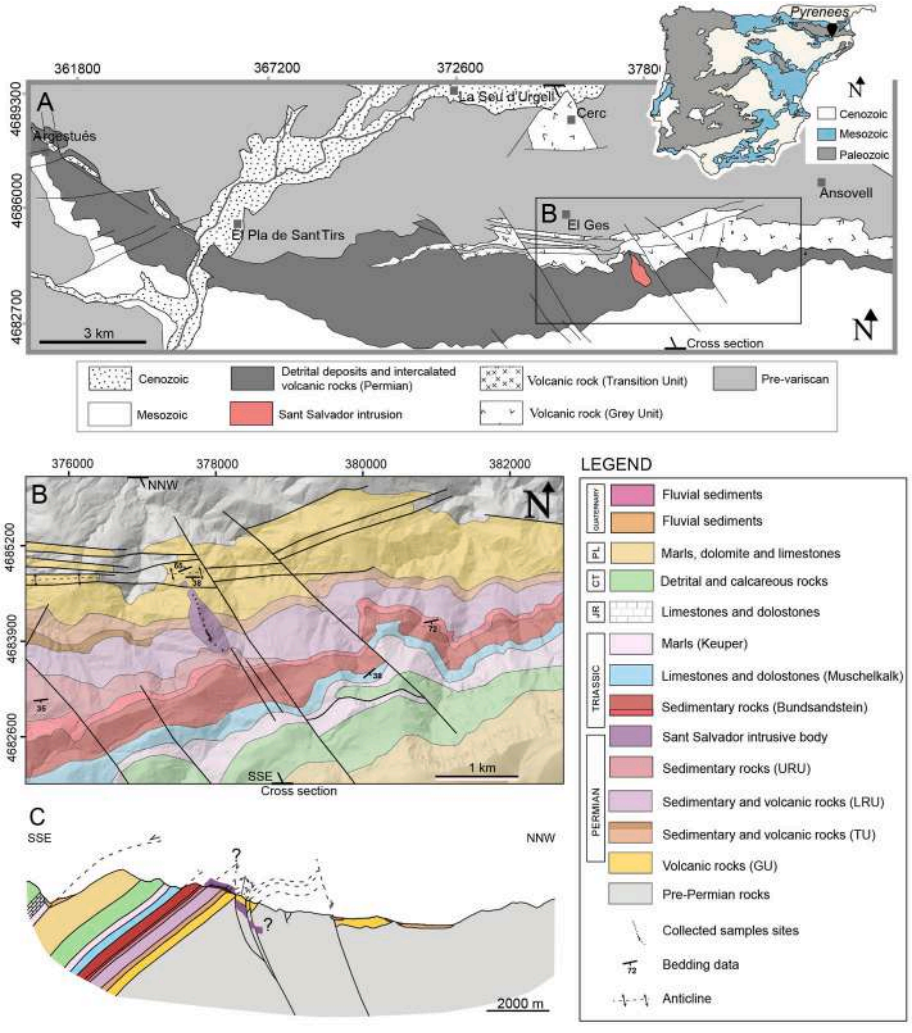

Fig. 1. A) Geological map of the Late Carboniferous-Permian basin, (modified from Gisbert, 1981); B) Detail of the location of the Sant Salvador intrusion (modified from Gisbert, 1981); C) Cross section of the Cadí basin. In purple, Sant Salvador intrusion and interpretation of its geometry and possible situation. A detailed location of collected samples sites is shown in Fig.6 and 7fig7. (For interpretation of the references to color in this figure legend, the reader is referred to the Web version of this article.)

From older to younger: Grey Unit (GU), Transition Unit (TU), Lower Red Unit (LRU) and Upper Red Unit (URU). The sedimentary sequences in the GU and TU pass laterally to pyroclastic rocks with interbedded lavas that in the GU are andesitic and, in the TU, dacitic (Gisbert, 1981). In the LRU and URU, siltstones, sandstones and red conglomerates alternate with interbedded volcanic bodies. Bixel (1984), based on geochemical criteria, established 5 volcanic episodes, the first three occurred during the sedimentation of GU, TU and LRU respectively, and episodes IV and V are linked with the URU. In the Cadí basin, Episode IV is only represented by the calc-alkaline andesites in the Sant Salvador intrusion. Based on facies analysis, cartography and geochemistry, previous authors interpreted that the Sant Salvador body intruded before the deposition of the URU, postdating the late Carboniferous-Permian andesites, but it is never intercalated in the LRU and URU (Gisbert, 1981; Bixel, 1984).

The Sant Salvador intrusion is relatively homogeneous and presents a trachytic aphyric grey texture, occasionally porphyric (less than 5% in volume, Bixel, 1984). Holocrystalline types are also recognizable in the "inner" part of the body (Lago et al., 2004). In its upper part, malachite mineralizations are common (Bixel, 1984) and edaphic alteration evidence its surface exposition before the deposition of the overlying succession.

Noteworthy, in most of the Sant Salvador body, the original mineral assemblage is strongly altered, as shown by the replacement of ferromagnesian silicates by chlorite and opaque minerals, and of plagioclase by sericite and carbonates. The geochemical study carried out by Lago et al. (2004), shows that plagioclase (almost pure albite, Ab>96) and clinopyroxenes, showing a wide compositional range, dominated the original assemblage. The IV episode, in which the Sant Salvador intrusion is included (Bixel 1984; Lago et al., 2004), together with Episode V, shows rocks with higher values of $Na_2O + K_2O$ respect to the previous episodes and a wide variation in the Nd-Sr isotopic compositions. This points to an abrupt change in the magma sources, from the crust (dominant in the three previous stages) to the lithospheric mantle, and also to the participation of enriched lithosphere and asthenosphere (possibly associated with a mantle plume) components in varying proportions. This compositional change reflects the evolution from the late Variscan transtensional tectonic regime to an extensional tectonic regime that induced mantle upwelling and decompression melting (Lago et al., 2004).

The Sant Salvador intrusion is a key element for deciphering the relationships between sedimentation and magmatism in the Permo-Carboniferous basins, despite the discrepancies regarding its origin and disposition. It has been described as 1) an intrusive body emplaced along a N140 fracture and characterized by a massive texture (without a jointing pattern) in its edges with a columnar disjunction tilted towards the South in its inner part (synchronous with the Upper Red Unit or slightly postdating it, Gisbert 1981); and 2) as a dyke with a N160-170 strike, and dipping 60-70°W as a consequence of the Pyrenean compression; this dyke would be several tens of meters thick, and would show columnar jointing with axes parallel to its walls (Bixel, 1984). The work by Bixel (1984) recognizes a system of minor dykes, 10 m thick and oriented N010 to N030 and considers the main intrusion tilted 45° following an E-W horizontal axis during the Pyrenean compression. Gisbert (1981) and Bixel (1984) describe a sinistral displacement of the segments of the structure, caused by either N70 fractures (Gisbert, 1981) or E-W faults (Bixel, 1984). The aim of this paper is to shed light on the origin and orientation of the Sant Salvador intrusion by means of the study of its magnetic fabric and microstructural and image analyses. Understanding the relationship between the magnetic fabric, the petrofabric of the rock and columnar jointing, and their variations along the igneous body is not only useful to characterize the Sant Salvador intrusion but also for establishing the basis for the application of these techniques to similar examples in the geological record elsewhere.

3. Methodology

3.1. Sampling campaign and laboratory procedures

A total of 20 sites, totaling 293 specimens, were sampled for the AMS and structural study. Sites are homogeneously distributed (average spacing between sites 50 m) in a NNW-SSE transect along the ridge of the intrusive body, depending on the accessibility of suitable outcrops (see Geological map in Fig. 1 and detailed sampling sites location in Figs. 6 and 7).

Samples were obtained in the field with a gasoline-powered drill. Six to 10 cylindrical cores per site were obtained. Cores were oriented in situ with a magnetic or a solar compass and sampling localities were positioned with a GPS. Oriented cores were cut to 2.1 cm-long, 2.5 cm-diameter standard cylinder specimens using a radial saw (non-magnetic steel) in the laboratory. Nine to 26 standard cylinder specimens were obtained in each sampling site.

The AMS measurements, its analysis and the interpretation of the magnetic fabric results from the initial 12 sampling sites (SS1 to SS12), which were later complemented with a second sampling campaign between sites SS3 and SS5. This resulted in eight new sampling sites (J1 to J8) to determine with higher accuracy the changes in the orientation of the magnetic ellipsoid axes.

3.2. AMS

Two types of analyses were conducted: 1) Anisotropy of Magnetic Susceptibility (AMS) measurements at room temperature (RT-AMS) for the 20 sites and 2) AMS at low temperature (LT-AMS) for 4 sites (J1, J8, SS8 and SS10These selected sites for LT-AMS are representative of different magnetic ellipsoids distributed in the lower, middle, upper and superficial zone of the intrusive body.

The AMS analysis was performed at the Magnetic Fabrics Laboratory of the University of Zaragoza, Spain, using a Kappabridge KLY-3S (AGICO Inc, Czech Republic). AMS is a technique that allows to define the spatial variation of the magnetic susceptibility (k) by applying a low intensity magnetic field (300 A m^{-1}) in different orientations around a standard specimen. Magnetic susceptibility (k) is a dimensionless proportionality constant (in the S.I. system) that indicates the relationship between an applied magnetic field (H) and the induced magnetization (M) of a rock; $M = k \cdot H$. AMS can be expressed mathematically as a second-rank symmetric tensor and geometrically as a magnetic ellipsoid with three orthogonal principal axes $K_1 > K_2 > K_3$. The magnetic susceptibility value (k) is the summation of the contributions of all the mineral species present in the sample and it depends on their spatial orientation within the analyzed rock. These minerals can exhibit one of the magnetic behaviors of matter: diamagnetic, paramagnetic or ferromagnetic s.l.

The magnetic susceptibility ellipsoid was described in detail by Nye (1957) and it is mainly characterized by three parameters (Jelinek, 1981): (1) the mean susceptibility (Km or Kmean), expressed as $Km = (K_1+K_2+K_3)/3$, (2) the corrected anisotropy degree (Pj) expressed as $\ln(Pj) = \sqrt{2((\ln(K_1/K))2 + (\ln(K_2/K))2 + (\ln(K_3/K))2)1/2}$, and (3) the shape parameter (T) expressed as $T = 2(\mu_2 - \mu_3)/(\mu_1 - \mu_3) - 1$ where $\mu_1 = \ln K_1$, $\mu_2 = \ln K_2$, $\mu_3 = \ln K_3$ y $\mu m = (\mu_1 + \mu_2 + \mu_3)/3$; that allows to distinguish between oblate (s.l.) ellipsoids, triaxial ellipsoids and prolate (s.l.) ellipsoids. There are two relevant features related to the magnetic susceptibility ellipsoid: 1) the magnetic lineation, that is the cluster of the K_1 axes and 2) the magnetic foliation, the plane whose pole is the set of K_3 axes.

The paramagnetic behavior is exponentially enhanced at low temperatures according to the Curie-Weiss law: $Kp = C/T - \theta$; Kp is the paramagnetic susceptibility, C is a constant and θ is the paramagnetic Curie temperature (Tc). In the LT-AMS analysis, to isolate the paramagnetic subfabric from the total fabric, four sites (J1, J8, SS8 and SS10) distributed along the different zones of the intrusion and the four groups

of magnetic fabrics (six specimens per site, but only four in one case), were analyzed. A thermal insulation was integrated around the measuring coil to thermally protect the instrument from the cooled samples (~77 K). The low-temperature-AMS (LT-AMS) measurement routine includes an 1-h cooling of the samples at 77 K by immersion in liquid nitrogen and measurements in the 15 manual positions. Between each position, the analyzed specimen was immersed again 1 min in liquid nitrogen.

The AMS results were processed and represented using: 1) the software *SUSAR* (AGICO Inc, Czech Republic) for the RT-AMS, 2) the software SUSAM (AGICO Inc, Czech Republic) for the LT-AMS and 3) the software *Anisoft 5.1.03* (Chadima and Jelínek, 2019) for the representation of all the AMS data.

The data obtained from both RT- and LT- AMS analyses were corrected to the horizontal taking into account the Permian red beds orientation (dip direction/dip, 170/44).

Density was measured for 237 specimens to investigate if there is a relationship between this property and the magnetic susceptibility or if there is a variation of density along the intrusion. For this purpose, for each specimen, dry weight and subsequently its weight immersed in water were measured. The density value of a standard specimen, was calculated according to Archimedes' principle, ρ = dry weight/(dry weight-weight immersed in water).

3.3. Rock magnetism

To elucidate the magnetic mineralogy, four temperature-dependent susceptibility curves, six hysteresis loops and three Lowrie's test or three-axis IRM demagnetization (Lowrie, 1990) were performed.

The four temperature-dependent susceptibility curves were analyzed in the KLY-3S Kappabridge with a CS-3 furnace at the University of Zaragoza (Spain), using the *software* SUSTE (AGICO Inc., Czech Republic). These analyses encompassed a range of temperature between 40 and 700 °C performed in an argon atmosphere in order to avoid mineral oxidations during heating. Samples J2-5, J7-2, SS8-5 and SS1–5B were selected according to their susceptibility values (K_m) as representative samples. These samples were powdered in an agate mortar (0.3–0.6 g per sample). Results were interpreted with the *software* Cureval 8 (Chadima and Hrouda, 2012) taking into account: (1) correction of the free furnace (measure of the CS3 without the sample), and (2) the normalization of the susceptibility values to a standard-volume specimen (calculating the density and the mass of the powder).

The hysteresis loops were performed in a QD (Quantum Design) MPMS XL (Magnetic Properties Measurement System) with a SQUID sensor magnetometer system at the University of Zaragoza (Spain) that allows to characterize the magnetic properties of a material. Samples SS2–4B, SS8–6B, SS10-6A, J1-2A, J3-3A and J7-2 were selected for having the highest susceptibility values (K_m) of the studied sites. They were powdered in an agate mortar (0.2–0.3 g per sample) and were measured at 300 K with an applied magnetic field that oscillates between 0 and 1 T. First in increasing field then in decreasing field up to a value 0 and later in the same way but with a negative value field. The hysteresis loops were analyzed by means of the *HystLab* software package (Paterson et al., 2018). A bulk measurement of each pulverized sample was made in the KLY-3S Kappabridge to check that the ferromagnetic mineral content is representative. Powdered samples were introduced in a diamagnetic gelatin capsule. Measurements routine includes a purgation of the sample, a calibration of the equipment and programming the points of measurement.

The three-axis IRM demagnetization also known as Lowrie's test or thermal demagnetization of the composite IRM (Lowrie, 1990) allows to identify the different mineralogical groups according to their coercivity value and the unblocking temperatures of magnetization by the induction of three IRM, one for each axis of the sample, in a decreasing order: 1.2 T (axis z), 0.3 T (axis y) and 0.1 T (axis x), respectively) and subjected to thermal demagnetization. The Lowrie's test was carried out for samples SS2-1, J1-1 and SS8-8 and IRM's were acquired with a IM10-30 (ASC Scientific) and measured with a JR6A (AGICO) at the Paleomagnetic Laboratory CCiTUB-Geosciences Barcelona (Geo3Bcn) (Spain).

3.4. Microstructural and image analyses

The microstructural study in oriented thin sections allows to determine the relationship between the orientation of the magnetic ellipsoid axes and the petrofabric of the rock (preferred mineral orientations or structures, mainly plagioclase). This study was done once the AMS data were analyzed and interpreted. It was carried out in five sites (J3, J6, SS2, SS8 and SS12) selected according to: 1) their position along the intrusive body axis, and 2) the orientation of the magnetic ellipsoid. Taking into account the magnetic fabric results, for each selected site, two mutually perpendicular thin sections were performed: 1) one of them contains the K_1 and K_3 axis of the magnetic ellipsoid and is perpendicular to the K_2 axis, 2) the other thin section contains K_2 and K_3 axis and it is perpendicular to the K_1 axis. As proposed in previous works (Oliva-Urcia et al., 2012; Simón-Muzás et al., 2022, among others) magnetic fabrics analysis has revealed a very useful tool for guiding in the definition of the optimal cuts to be studied under the microscope.

Due to the aphanitic texture of the rocks, that prevents the determination of the texture in outcrop observations, mineral orientations were studied in 10 thin sections by means of the following routine: (1) inspection and manual measurement in an optical microscope under transmitted light and high-resolution image analysis from clean binary files (black color for the particles and white for the background) in order to analyze their shape and orientation by means of (2) *ImageJ* software (Schneider et al., 2012) that allows to obtain histograms of the angle of the long axis of a set of particles with respect to an horizontal line; and 3) Intercepts *software* (Launeau and Robin, 1996) that is based on counting the number of intercepted segments of a set of objects on the image by a set of parallel scan lines along a number of directions. From this, a rose diagram that shows the number of intersections in each direction is obtained allowing to determine the petrofabric.

4. Results

4.1. Field observations

Although the contact with the URU is not well exposed due to the dense Scots pine forest that surrounds the intrusion, a reddish breccia, that is mainly composed by clasts from the preVariscan basement and the volcanic units underlying the Sant Salvador intrusion, covers the rubefacted uppermost rocks of the intrusion. The breccia is recognizable below the reddish polygenetic microconglomerates and sandstones from the URU (Fig. 2A). The top of the intrusive body is characterized by an edaphic profile with a rubefacted bedrock overlain by a regolith in conformity with the beds of the URU. The rocks from the Sant Salvador body are strongly fractured. The dominant set shows a NNW-SSE trend with dips between 45° to 90° towards the West (average attitude of the Sant Salvador intrusion). In the middle part, between sites SS6 and SS9, fracturing is arranged as a columnar jointing (Fig. 2B) in which the dominant set represents one of the long faces of the columnar jointing. The second joint family shows a NE-SW trend with dips between 30° and 90° towards the NW. The third set, less represented, shows an E-W trend with dips between 40° and 50° towards the S, parallel to the bedding of the URU, and represents the bases of the prisms. The fourth set shows a NW-SE orientation dippin g about 50-70° towards de NE and also consistent with columnar fracturing. Weathering has originated the individualization of some of the prisms and rockfall, generating a rocky ground around the ridge.

Taking into account the bedding data of the URU and the reddish breccia surface (N90 to N110 strike tilted 40° to 50° towards the South), the restored columnar jointing (intersection of planes, and therefore axes of columns) is oriented close to the vertical. The present-day

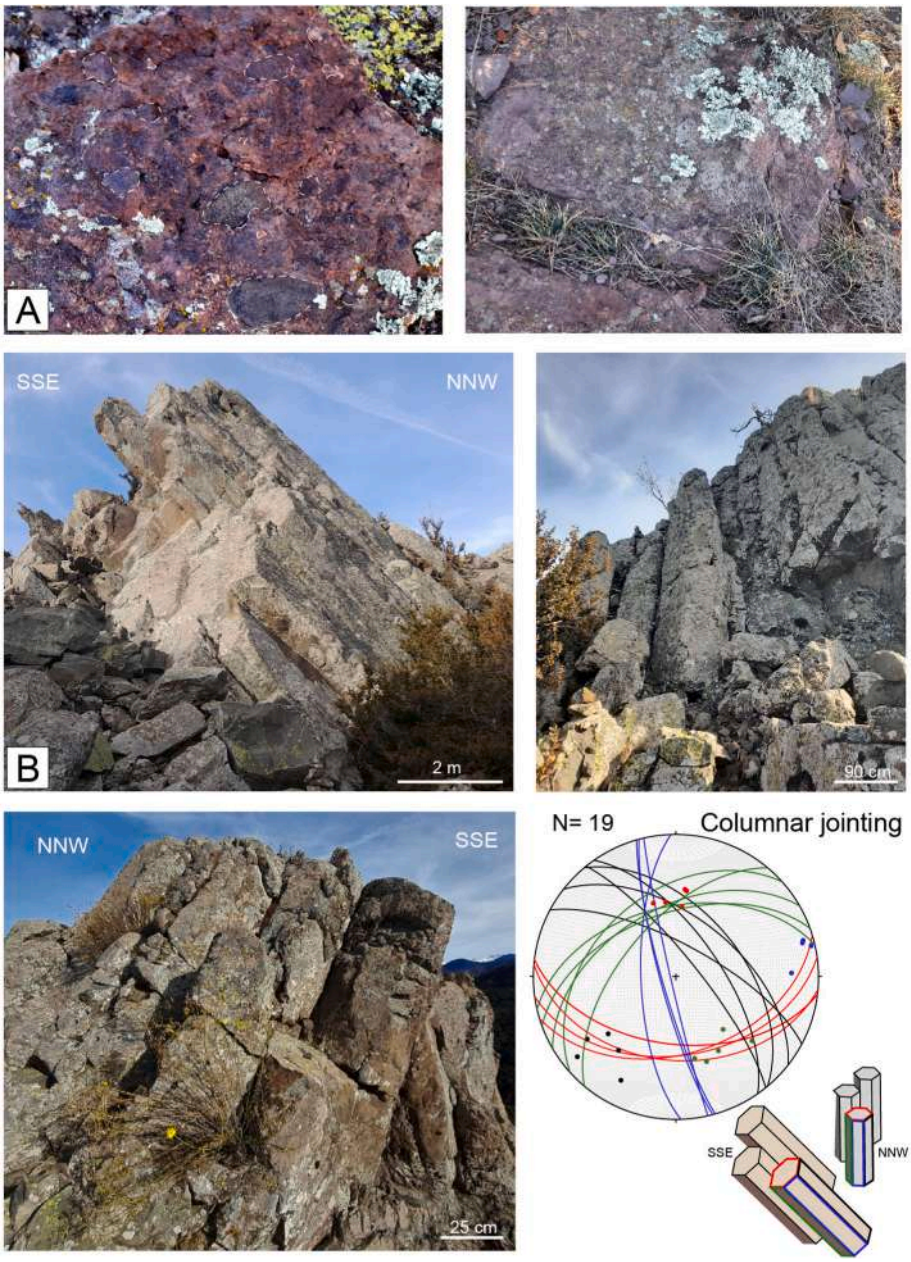

Fig. 2. A) Views of the reddish breccia (some clasts are outlined to highlight lithologies and sizes (left) and URU sedimentary red beds (right) in the contact with the intrusive body; B) Different views of the columnar jointing developed in the middle part of the Sant Salvador intrusion and stereoplot (lower hemisphere) of the joint sets in situ. (For interpretation of the references to color in this figure legend, the reader is referred to the Web version of this article.)

average orientation of the prisms from the columnar jointing is about 355/45 (Fig. 2B).

4.2. Magnetic mineralogy and rock magnetism

All temperature-dependent susceptibility curves are irreversible (the heating and cooling curves present different paths), and they show a consistent decrease and increase in the susceptibility value at 580 °C in the heating and cooling run respectively. The heating curves (Fig. 3A) show an increase between 0 and 300 °C and a strong drop between 320 and 380 °C. The abrupt drop in the heating curve at 580 °C suggest the presence of magnetite and the increase at the same temperature in the heating curve, points towards the neoformation of a ferromagnetic phase. This ferromagnetic neoformation generates the irreversibility of the curves. The increase and then the strong drop in susceptibility between 0 and 380 °C in the heating curve indicates the presence of titanomagnetite/titanomaghemite with unstable intermediate phases having different Ti concentration (see Diarte-Blasco et al., 2020). Sample SS1–5B, the site closest to the paleosol, presents a slight decay at 670 °C close to the Néel temperature of hematite (670 °C) what indicates the presence of this mineral. Thus, the temperature-dependent magnetic susceptibility curves suggest the predominance of magnetite and titanomagnetite/titanomaghemite as ferromagnetic mineral in most samples (i.e. sites with Km values higher than $600{\cdot}10^{-6}$ SI) and the predominance of hematite in site SS1 with a Km site mean below this value (Table 1).

The hysteresis loops of the studied samples (Fig. 3B) show, in the raw data, (before slope correction) a paramagnetic contribution to the total magnetic behavior (SS2–4B, J7-2, SS10-6A). This paramagnetic contribution is less important in samples J3-3A, J1-2A, SS8–6B. In all the samples, the hysteresis loops are narrow and reach complete saturation before 1 T. This can be interpreted as resulting from the presence of low

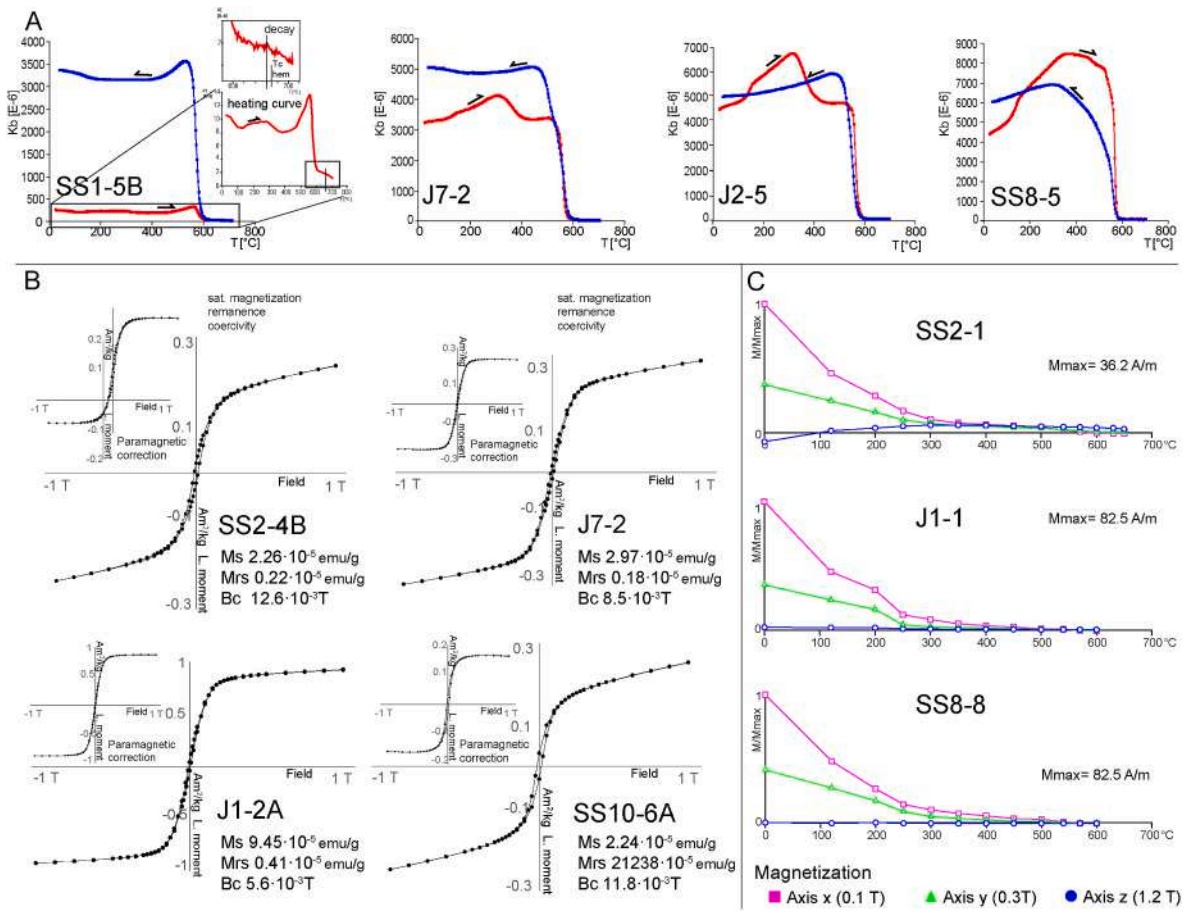

Fig. 3. A) Temperature-dependent susceptibility curves (40–700 °C) of heating (in red) and cooling (in blue) for the four analyzed curves, where the non-reversibility of curves can be observed; B) Representative hysteresis loops before and after paramagnetic slope correction. Values of Ms: magnetization saturation, Mrs: coercive force, Bc: coercivity of remanence obtained with HystLab software (Paterson et al., 2018); C) Lowrie's test, IRM demagnetization along three axis X: 0.1 T, Y: 0.3 T and Z: 1.2 T. (For interpretation of the references to color in this figure legend, the reader is referred to the Web version of this article.)

Table 1
Magnetic parameters (AMS) for the sampling sites in the Sant Salvador intrusion.

Site	N	Km (10^{-6})	e (10^{-6})	K_1 in situ	Conf. Ang.	K_3 in situ	Conf. Ang.	Pj	e	T	e
SS1	10	592	396	088/14	12/07	182/15	12/08	1.027	0.008	0.365	0.267
SS2	14	2695	490	258/08	13/04	348/04	05/04	1.037	0.005	0.728	0.1
SS3	14	1897	893	078/21	14/05	170/04	06/04	1.041	0.002	0.564	0.084
J8	12	2153	750	080/27	14/05	350/0	11/05	1.032	0.004	0.552	0.125
J7	13	4738	1230	078/31	06/03	343/08	07/05	1.046	0.008	0.421	0.117
J6	14	3891	2097	063/39	10/07	159/07	08/06	1.041	0.008	0.592	0.103
J5	12	2621	577	060/45	07/03	157/07	04/03	1.035	0.003	0.44	0.058
SS4	9	2056	1340	071/40	30/11	338/04	15/07	1.026	0.008	0.367	0.176
J4	10	6653	3389	038/53	26/09	143/12	17/07	1.032	0.013	0.398	0.248
J3	14	8319	3245	023/67	16/05	145/13	13/08	1.04	0.012	0.265	0.236
J2	24	8864	4443	285/36	37/32	100/54	62/23	1.03	0.015	0.244	0.346
J1	16	15870	2652	03/63	10/05	139/20	13/03	1.052	0.011	0.079	0.096
SS5	11	14770	1906	02/53	11/02	134/27	06/02	1.053	0.007	0.219	0.228
SS6	13	673	534	357/43	13/04	154/44	10/07	1.018	0.004	0.21	0.314
SS7	13	10360	8	344/18	07/05	129/68	16/05	1.037	0.02	0.256	0.242
SS8	26	10640	3846	336/38	17/07	128/48	19/05	1.035	0.009	−0.058	0.262
SS9	17	1053	625	320/8	29/22	078/73	29/17	1.013	0.01	0.051	0.335
SS10	22	1218	931	287/37	17/08	130/51	09/08	1.014	0.005	0.475	0.28
SS11	9	2448	2652	313/58	14/09	190/19	13/07	1.032	0.015	0.432	0.213
SS12	19	2831	1998	319/42	14/08	181/39	12/06	1.036	0.016	0.289	0.179

N: number of specimens; K_1 and K_3-mean (trend and plunge) of the magnetic lineation and of the pole to the magnetic foliation (Jelinek, 1977) in situ; Conf Ang: major and minor semi-axes of the 95% confidence ellipse (Jelinek, 1977); Km: magnitude of mean magnetic susceptibility (10^{-6} S.I); Pj: corrected anisotropy degree (Jelinek, 1981); T shape parameter (Jelinek, 1981); e: standard deviation.

coercivity ferromagnetic minerals such as magnetite, as also indicated by the three-axis IRM demagnetization. According to the basic hysteresis loop shapes that may help to identify the magnetic phase (Tauxe, 2008), superparamagnetic (samples J1-2A and J7-2) and pseudo-single domain (J3-3A. SS2–4B, SS8–6B and SS10-6A) magnetite may be present but multidomain magnetite (MD magnetite) cannot be discarded.

According to the three-axis IRM demagnetization (Fig. 3C), samples show a certain amount of magnetization in the minimum and intermediate axes (x and y axes) where 0.1 and 0.3 T were applied, respectively) and is minimum in the maximum field axis (z axis 1.2 T applied), pointing to an absence of high coercivity minerals in these samples. There is an abrupt decay in the magnetization value in the minimum and intermediate axes of the three analyzed samples at 250–300 °C, which can be related to the presence of titanomagnetite with a high content of Ti (around 40–50%). Finally, a slight decay is observed in the IRM curves at 580 °C which is the unblocking temperature of magnetite. The presence of multidomain magnetite is not discarded.

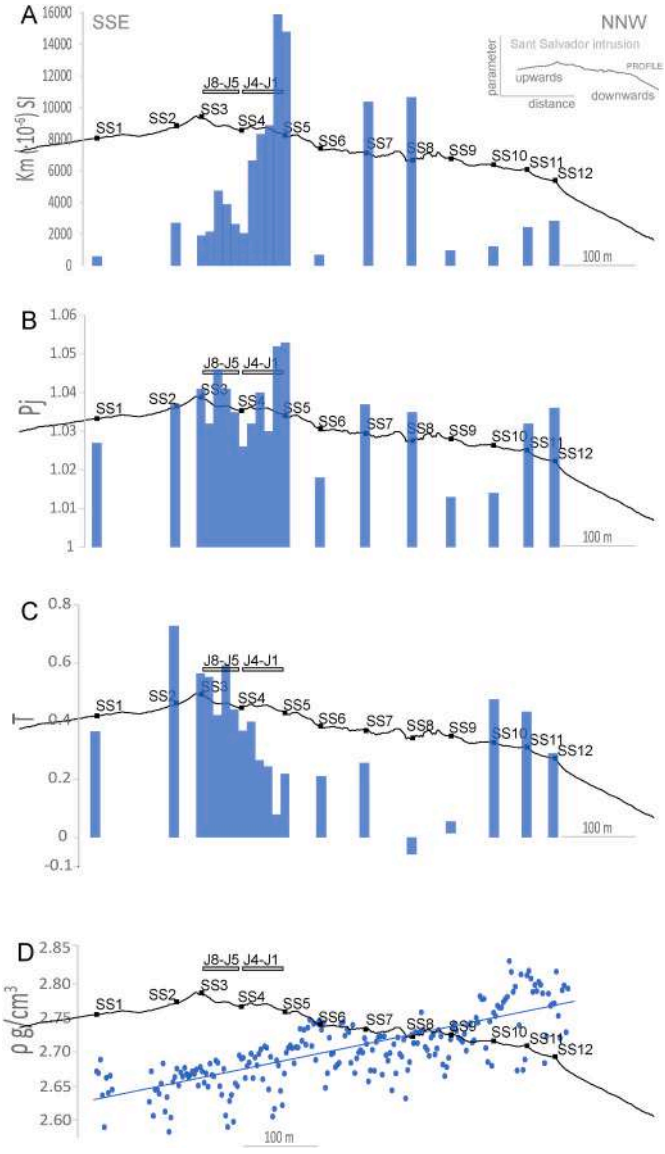

Fig. 4. Mean value per site of the magnetic parameters of the magnetic susceptibility ellipsoids throughout the sampling section in the Sant Salvador intrusion: A) mean susceptibility, B) corrected anisotropy degree (Pj), C) shape (T) and D) density (g/cm3). In black color studied sites along the ridge.

4.3. Magnetic susceptibility and density values

The mean value of the magnetic susceptibility (Km) is $5217 \cdot 10^{-6}$ SI, ranging between $592 \cdot 10^{-6}$ SI (site SS1) and $15870 \cdot 10^{-6}$ SI (site J1). The highest values of Km appear in the middle part of the intrusion except for site SS6 (Fig. 4A, see Table 1 for magnetic parameters data). Most sites display Km site mean values higher than $1000 \cdot 10^{-6}$ SI, also suggesting that the main carriers of the AMS are ferromagnetic minerals (see Knight and Walker 1988; Hargraves et al., 1991; Rochette et al., 1991). The contribution of diamagnetic (plagioclase and other feldspars) and paramagnetic grains (i.e. olivine, pyroxene, hornblende) to the total anisotropy can be considered low (as also inferred from LT-AMS measurements).

The values of the Pj parameter range between 1.013 and 1.053. The lowest degree of anisotropy, Pj, is present in two adjacent sites (SS9 and SS10) located at the top of the lower part of the intrusive body (Fig. 4B). Regarding the shape of the magnetic susceptibility ellipsoids, most sites show an oblate magnetic fabric with values of T above 0.2, except site J1 (T = 0.079). site SS8 (T = -0.058) andsite SS9 (T = 0.051), which show a neutral triaxial shape (Fig. 4C). The polar Pj-T plot shows a dominance of oblate magnetic fabrics at site level and at specimen level, with a low to medium degree of anisotropy (Fig. 5A and B). At site level, magnetic parameters show some correspondence between Pj and Km on one side and T and Km on the other. The Pj and T parameters decrease with increasing Km with a low correlation coefficient, Fig. 5 C, D), indicating that the higher the content in ferromagnetic carriers, the lower the oblateness of the ellipsoids. There is neither correlation between Km and Pj (Fig. 5 D) nor a relationship between the preferred orientation of the magnetic susceptibility ellipsoid axis and the magnetic parameters (Km, Pj and T).

The density of the studied rocks (Fig. 4D) shows a maximum value of 2.83 g/cm^3 and a minimum value of 2.58 g/cm^3, thus indicating a strong variability for similar rock types. At site level, density values compared with magnetic parameters (Pj, T and Km) do not show any relationship. However, when density values are represented along the sampling profile, they show a progressive increase towards the NNW (Fig. 4D). This means that there is a gradient of increasing density from the upper part toward the lower part of the intrusion.

4.4. Magnetic fabrics

The AMS results show a good clustering of the magnetic ellipsoid axes with the exception of site J2, that presents an anomalous magnetic ellipsoid with high degree of dispersion of its axes (Fig. 6). For that reason, this site has been excluded in further interpretations.

After bedding restoration, the orientation of the magnetic ellipsoid axes is as exposed below. All positions are referred to the edaphic breccia located in the upper part of the intrusion:

- In the lower part (sites SS12, SS11, SS10, SS9), the magnetic lineation (K_1) progressively changes its orientation from the lowest site (SS13) to near the middle part (SS9) from a N258 to a N307 trend. The plunge changes from 67° to 43° towards the NNW.
- In the middle part of the intrusion (sites SS8, SS7, SS6, SS5, J1, J3 and J4), the magnetic lineation (K_1) presents a vertical or subvertical orientation The inclination changes along the transect, between 85 and 62°. Site J3 marks the trend for the next group of magnetic fabrics of the upper part.
- In the upper part (sites J4, SS4, J5 and J6), following the previous trend, the magnetic lineation (K_1) presents an orientation that gradually changes to N109 –N100. The inclination changes progressively between 59° to 33° towards the E.
- In the uppermost part, close to the paleotopography (sites J7, J8, SS3, SS2 and SS1), the magnetic lineation (K_1) presents an orientation around N095 and finally becomes subhorizontal, following the previously described trend.

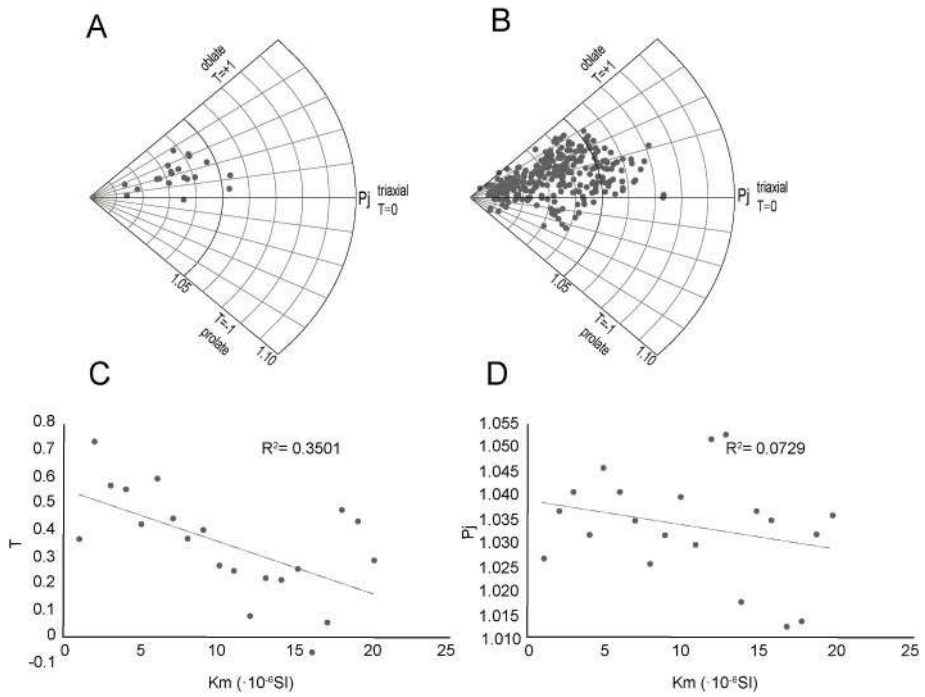

Fig. 5. A) Polar Pj-T plot (sampling sites means value). B) Polar Pj-T plots (data from specimens from each studied sites). C) Km-T diagram, D) Km-Pj diagram.

Considering the overall trend of the K_1 axes, a gradual change on their orientation is observed from the bottom to the top of the body (according to the relative position in relation to the stratigraphic succession), from 258 (intermediate to steep plunges) to 095 (subhorizontal) along the position of the intrusive body in the stratigraphic succession.

In this sense, four groups of magnetic fabrics can be distinguished according to the orientation of the magnetic lineation before and after bedding correction (Table 1 and Figs. 6, 7) along the four parts of the intrusive body with different position (i.e. depth after bedding restoring) in relation to the stratigraphic succession.

Regarding LT-AMS results (Fig. 8), the Km-LT/Km-RT ratio per site ranges between 0.83 and 1.94, indicating the dominance of the ferromagnetic behavior in the contribution of the magnetic fabrics. The paramagnetic contribution is small. In all the analyzed sites, the LT-AMS results show that the magnetic fabrics axes are clearly scattered, not improving the signal of RT-AMS.

4.5. Microstructures and image analysis

The main textural elements in the studied samples are tabular plagioclases arranged in a trachytic texture, which show an average grain size of 320 μm. These mineral grains are parallel, imbricate and/or arranged in fans. In the studied samples they show a main preferred orientation except in sample SS12 where the alteration masks the original texture. When larger phenocrysts of plagioclase are present, small grains of plagioclases are reoriented around them. This phenomenon is also observed around a xenolith in thin section J6-9A (Fig. 9). Opaque minerals, that could correspond to ferromagnetic grains without a preferred orientation under the optical microscope, are also present.

The preferred orientation of plagioclases, detected in the two mutually orthogonal thin sections, allows to determine the (magmatic) foliation plane and to establish the relationship between this plane and the magnetic susceptibility axes. In all sites, plagioclase orientations (long axes of grains in thin section) are close or within the α95 confidence angle of the K_1 and K_2 magnetic ellipsoid axes. By means of the image analysis software (*ImageJ* and *Intercepts*) a secondary plagioclase orientation in an intermediate position or close to the K_3 axes was detected. In site SS12, which does not show a trachytic texture, the three techniques show that there is no preferred orientation of mineral grains. Besides, the eccentricity of the ellipse (Fig. 10) can help elucidate which of the two mutually thin sections approaches better the mineral lineation; eccentricity should be maximum when the cut is parallel to the mineral lineation and minimum when the cut is perpendicular to it, because in these samples the lineation is defined by the intersection of planar elements. However, in the studied examples, the differences are subtle, and results are not significant. The eccentricity is slightly higher in the section perpendicular to K2 for sites SS8, J6, and for sites J3 and SS2, it is higher in the section perpendicular to K_1. In the same way, the long axes of the particles are longer in the section parallel to the K_1 axis in sites J6, J3 and SS8 and in site SS2 this happens in the section parallel to the K_2 axis. Neither of the two parameters gives significant results in site SS12 due to the negligible differences in these values.

The presence of discrete bands defined by the disposition of certain plagioclase grains (Fig. 9), deflected with respect to the trend of the foliation, was recognized under the optical microscope, but not with the automated methods. Crystals are not broken or fractured, except for one thin section, that is not representative of most surfaces. In any case, the orientation of these bands, showing systematic sinistral and dextral shears, is bears no relationship with the magnetic ellipsoid axes.

5. Interpretation and discussion

5.1. Magnetic properties and magnetic carriers

An important issue in magnetic fabrics is the characterization of the magnetic carriers of the AMS. In the Sant Salvador body, most samples show high Km values, suggesting that the main carriers to the AMS are ferromagnetic minerals (see Knight and Walker 1988; Hargraves et al., 1991; Rochette et al., 1991). Among those, the temperature-dependent susceptibility curves indicate that probably magnetite, titanomagnetite/titanomaghemite and locally in the uppermost part of the intrusion, hematite are the main contributors. The hysteresis loops corroborate the presence of a low coercivity ferromagnetic mineral (eg. magnetite) and the three-axis IRM points toward magnetite with a high content in Ti due to the abrupt decay of the magnetization at 250-300 °C. The presence of

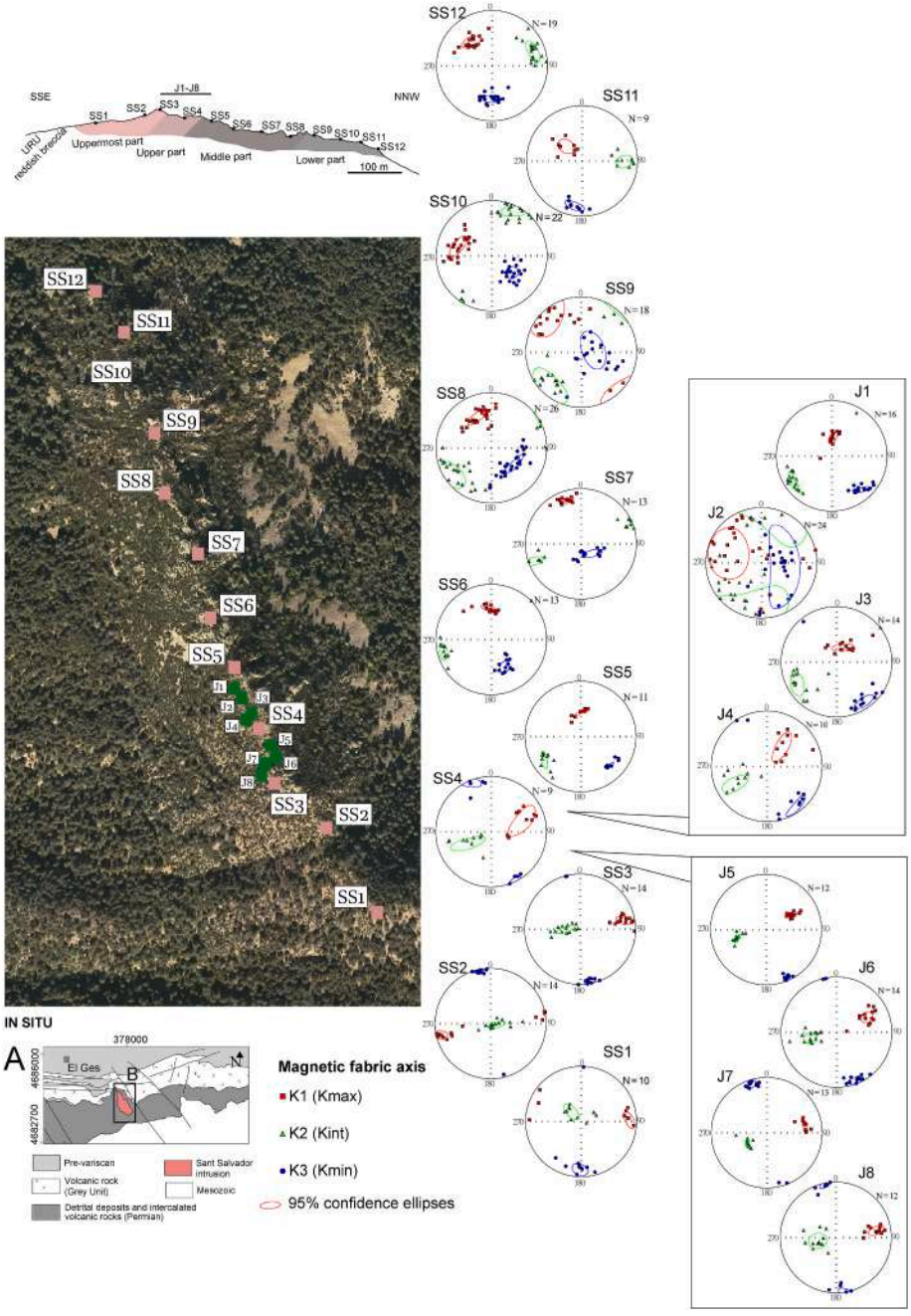

Fig. 6. A) Situation of the Sant Salvador intrusion, B) In situ, AMS ellipsoids obtained for each sampling site with 95% confidence ellipses (Jelinek, 1981) in the Sant Salvador intrusion.

iron sulphides is discarded because their characteristic decay is not observed in the temperature-dependent susceptibility curves. In the superficial zone, reddening of the rocks is due to an oxidation process by the proximity of the overlying red beds (URU) and hematite is likely a product of a lateritization under tropical climate and not a mineral from the original composition of the rock. It should be noted that the contribution of plagioclase (i.e. diamagnetic mineral), the most abundant mineral observed in thin sections, to the total magnetic anisotropy, can be considered negligible. Therefore, given the abundance of plagioclase and the very high Km values, the magnetic properties could arise from ferromagnetic exclusions around and/or within the plagioclase. This assumption, developed in depth in the next section, can be validated considering the parallelism between the foliation defined by the plagioclase orientations and the foliation plane of the magnetic ellipsoid which indicates that the ferromagnetic minerals are arranged with the same orientation as plagioclases. This explains why both the orientation of diamagnetic (plagioclase) and ferromagnetic (magnetite/titanomagnetite) minerals show the primary fabric of the rock, originated during the emplacement of the intrusion.

In the present study a difference between magmatic and magnetic fabric as noted in other cases (e.g. Hoyer, 2015) is not observed, probably because these differences are the result of a higher degree of rigid-body rotation due to the magma flow, preferentially in the elongate plagioclases instead of the fine-grained granular magnetite developed upon a fine-grained trachytic texture (see, e.g. Budkewitsch and Robin (1994) and Hetényi et al. (2012)). The notable variations of the mean value of magnetic susceptibility, ranging between $592 \cdot 10^{-6}$ SI (site SS1) and $15870 \cdot 10^{-6}$ SI (site J1) may be due to small-scale

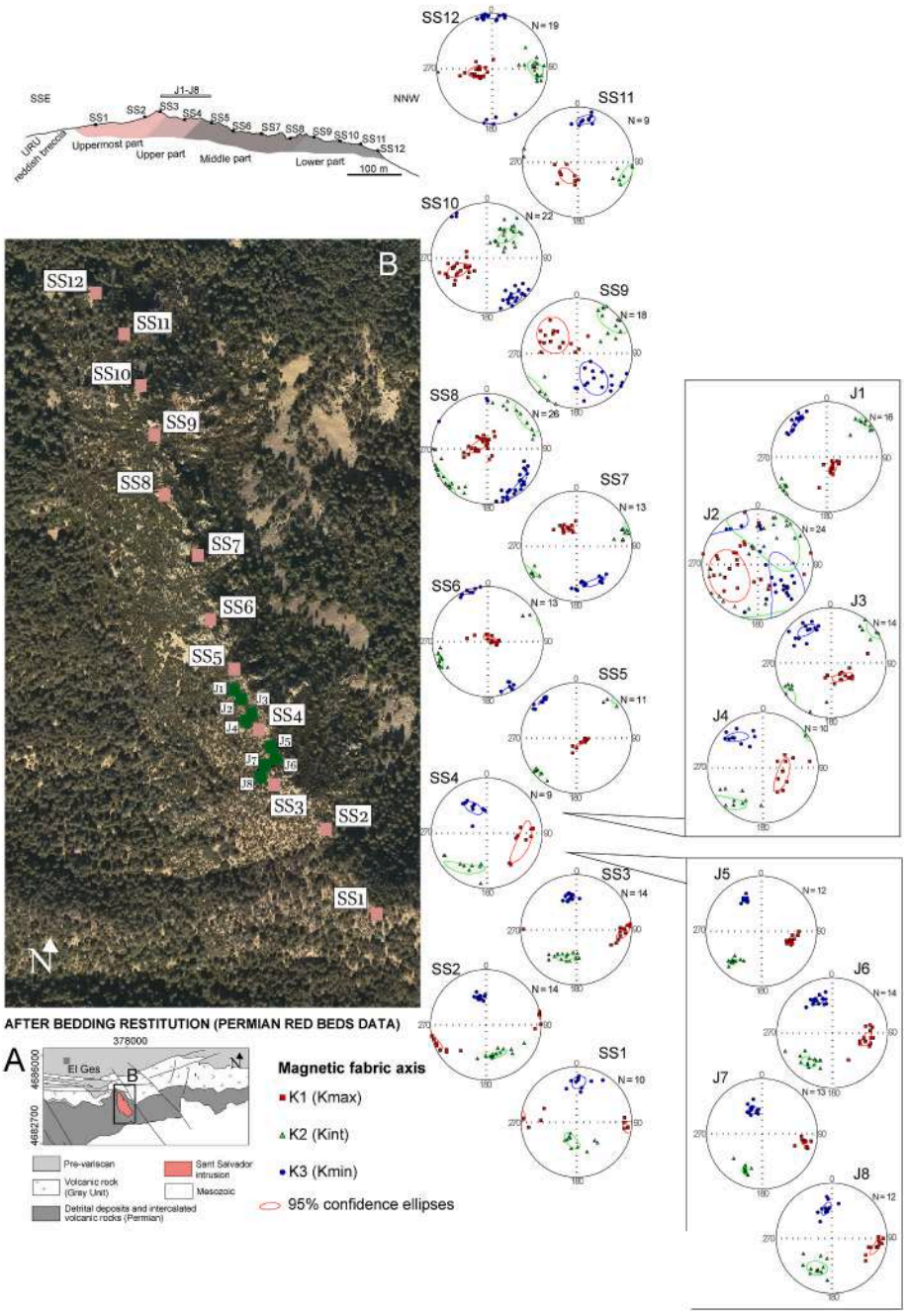

Fig. 7. A) Situation of the Sant Salvador intrusion, B) AMS ellipsoids obtained for each sampling site with 95% confidence ellipses (Jelinek, 1981) in the Sant Salvador intrusion after bedding restitution with bedding data from sedimentary Permian red beds. (For interpretation of the references to color in this figure legend, the reader is referred to the Web version of this article.)

enrichment in ferromagnetic minerals in the different parts of the intrusive body during its emplacement. The clear gradient in density values points towards decreasing iron content upwards in the intrusion, despite the fact that an opposite trend is observed in the Km value at site level. In any case, the mean value of susceptibility in the Sant Salvador body is higher (5217·10-6 SI) than that of the rocks that surround it: sedimentary red beds (296.49·10-6 SI) from the LRU and URU and volcanic and volcaniclastic rocks from the GU and TU (926.84 $\cdot 10^{-6}$ SI). This strong difference can be related to the different (mantellic) origin of the Sant Salvador intrusive body proposed by some authors (Lago et al., 2004) in relation to older volcanic rocks of the area.

5.2. Magnetic fabrics and petrofabric relationship

The observations under the optical microscope and the magnetic fabrics results (oblate ellipsoids) point towards a planar-linear rock fabric defined by planar elements. The overall K3 axis data, after restitution, yield a magnetic foliation that dips steeply towards the SSE. In all the studied samples, this magnetic foliation is parallel or subparallel to the foliation plane defined by the preferred arrangement of the plagioclases (Fig. 11). This indicates that, despite the fact that the petrofabric (the plagioclase microliths) does not directly condition the magnetic fabric, the ferromagnetic minerals that are the main magnetic carriers, are arranged consistently with the planes defined by the plagioclases as observed in other studies (Hargraves et al., 1991; Bascou et al., 2005).

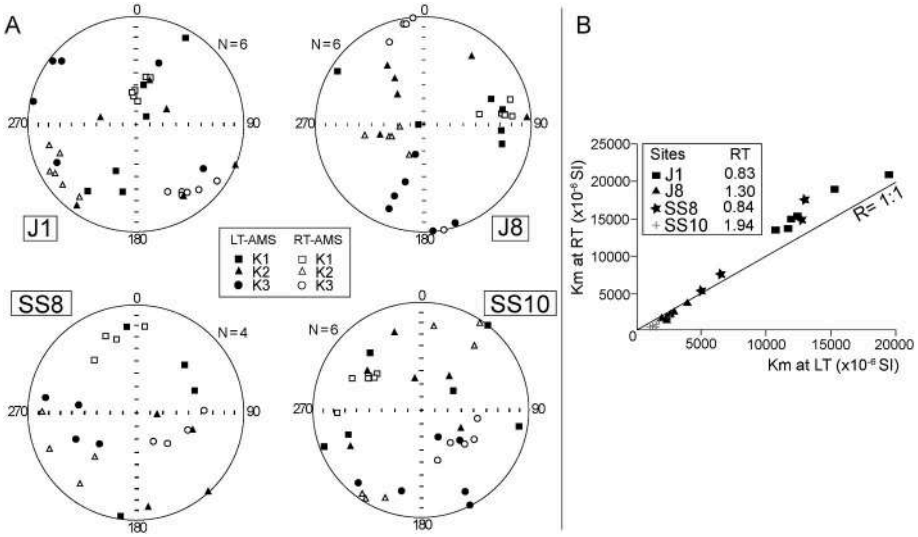

Fig. 8. A) Comparison between RT-AMS (white symbols) and LT-AMS (black symbols) for each sampling site. B) Ratio between the magnetic susceptibility at low and room temperature (LT/RT).

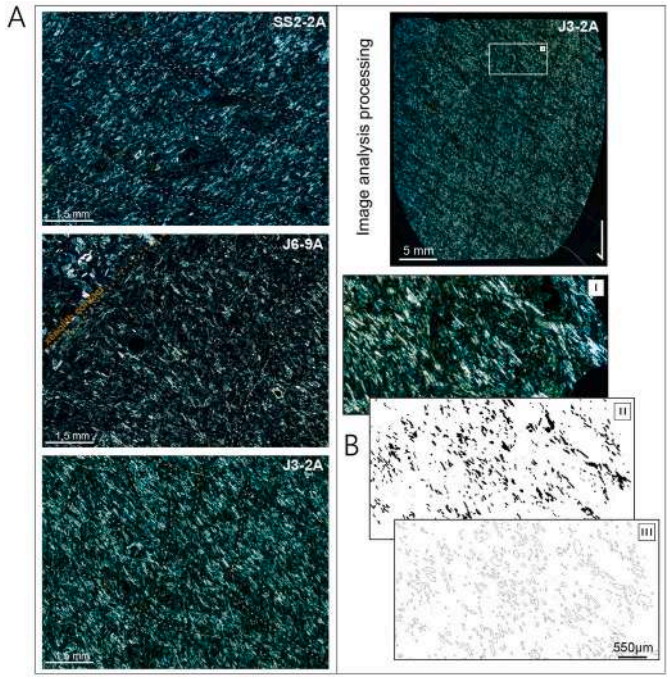

Fig. 9. A) Petrological details (under polarized light): trachytic texture, preferent orientation of plagioclases, reorientation of plagioclases at the edges of a xenolith, bands deflected with respect to the present foliation (in white dashed line); B) Example of an image analysis processing.

Another possibility is that ferromagnetic minerals are contained within the plagioclase grain and contribute to the magnetic fabric as has been observed in gabbronorites from the Bushveld layered intrusion (Feinberg et al., 2006) although in that case, it could not be determined if AMS fabric was due to alignment of interstitial magnetites, or to the alignment of silicate minerals and the exsolved magnetite inclusions within them. In another case, it is observed that in columnar jointing in basalt where internal structures are observed and are related to melt migration parallel to the column axis; the long axes of titanomagnetite crystal are parallel to the long axis of the basalt column (Mattsson et al., 2011).

In addition, observations that indicate that both plagioclase and ferromagnetic minerals present the same orientation and spatial distribution confirms that either a) ferromagnetic minerals have crystallized during the same process during the ascent of the magma flow towards the surface; or alternatively that b) in a subsequent process, they have been formed in the interior, interstices or crystal boundaries reproducing the orientation of the primary fabric. This last explanation has been also pointed out by Stacey (1960) in a dolerite sill, and experimentally tested by Hargraves et al. (1991), and also observed in a Quaternary lava flow by Bascou et al. (2005). Surface processes and rubefaction in the contact with the LRU or the sericitization of the plagioclases have not modified this magnetic fabric.

In relation to the fracture pattern generating columnar jointing (Fig. 12), it is remarkable that both the foliation defined by plagioclase and the magnetic foliation are parallel to the ENE-WSW fracture set. This supports that the foliation defined by the plagioclases is expressed as surfaces of weakness in the rock, defining preferential fracture surfaces. This behavior contrasts with most volcanic bodies, where joint geometry is directly conditioned by the geometry of the body and its walls (Hetényi et al., 2012; Hetényi and Milazzo, 2014), and in turn approaches those examples (Almqvist et al., 2012) in which jointing is closely related to the internal fabric of the rock. An alternative explanation would be the possibility of explaining the Sant Salvador intrusion as a tabular body parallel to bedding (in which case columnar jointing would be perpendicular to the body walls), but this geometry is difficult to conciliate with its internal fabric. In relation to the formation of columnar joints, it is observed that are developed in intrusive and extrusive volcanic rocks regardless their chemical composition or emplacement context. The formation of columnar joints only happens in an extremely rapidly cooling environment like in the fluid-saturated environments (Lamur et al., 2018). Previous studies (Lamur et al., 2018 references there in) point out that the time scales for magma cooling only considering conduction are longer than considering the infiltration and circulation of external fluids in the process. Therefore, columnar joints are formed and propagate in solid state at moderate-high temperatures, in a purely elastic regime of the rocks were the circulation of external fluids accelerates the cooling of the magma and accentuates heat exchange (Lamur et al., 2018).

Regarding the methodology used in the microstructural study, the thin section observations under the optical microscope show the best results for the determination of foliation plane of the rock (Fig. 11). The *ImageJ* and *Intercepts* softwares represent a good approximation of the preferred arrangement of minerals observed in the whole thin sections, but they also provide other directions that are not the result of a primary

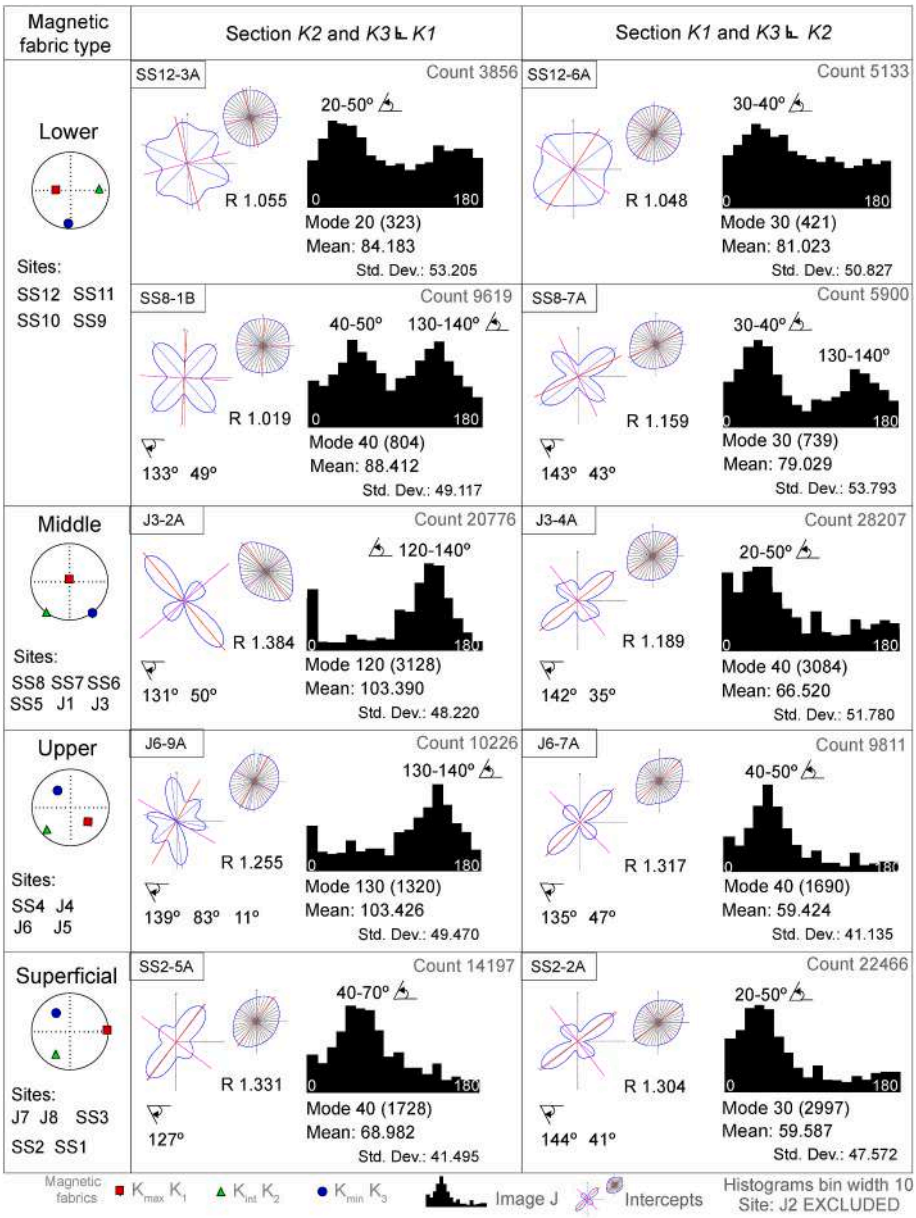

Fig. 10. High-resolution image analysis results in two mutually perpendicular thin sections per site, according to the four types of magnetic fabrics by means of 1) software ImageJ: histograms of angle of the long axis of the particles respect to an horizontal line, and 2) software Intercepts: diagram of traverses (resultant ellipse) and directions (resultant rose diagram).

preferential alignment of minerals but are rather artifacts resulting from by the interference caused by the deflection of the plagioclases by shear bands. These two processes resulting in primary and secondary orientations can only be distinguished by means of manual procedures. Therefore, in our case, the eccentricity of the ellipse and the orientation of long axes calculated by means of *Intercepts* and *ImageJ* softwares do not provide completely satisfying results. Qualitatively, it can be observed that in thin sections perpendicular to K_1 axis, grains are not so well oriented than in sections containing K_1 axis. This fact agrees with a planar-linear rock fabric, which explains the well-defined magnetic lineation despite being an oblate fabric.

As noted in the Results section, the site J2 presents an anomalous magnetic fabric with a high degree of dispersion of its axes and for that reason, it was excluded of the study. The temperature-dependent susceptibility curve does not show any magnetic contribution different from the rest of the sites. Neither does its position in the middle part of the intrusive body, nor does its magnetic ellipsoid parameters (Km, Pj and T) yield any information that clarifies the reasons for this anomalous magnetic fabric. The oriented thin section perpendicular to K_2 and containing K_1 and K_3, carried out to study in detail the distribution of the components of the petrofabric, does not show any remarkable difference in mineral content or distribution. In this thin section the three methods applied in the microstructural analysis show that, except for the preferred orientation detected with *Intercepts* software, plagioclase tend to get close to the K_1 axis. The orientation of K_1 is clearly different from the rest of the sites in the middle part. This change may reflect a local change in magma flow direction by a local disturbance.

The bands defined by the disposition of certain plagioclases that are deflected with respect to the foliation, seem to be generated by a late process during the cooling of the body, possibly at high temperature because no solid-state deformation seem to affect the plagioclase crystals. The existence of bands with different sense of shear also points to a tectonic origin under the regional or local stress field but they seem to be unrelated to the magnetic fabrics.

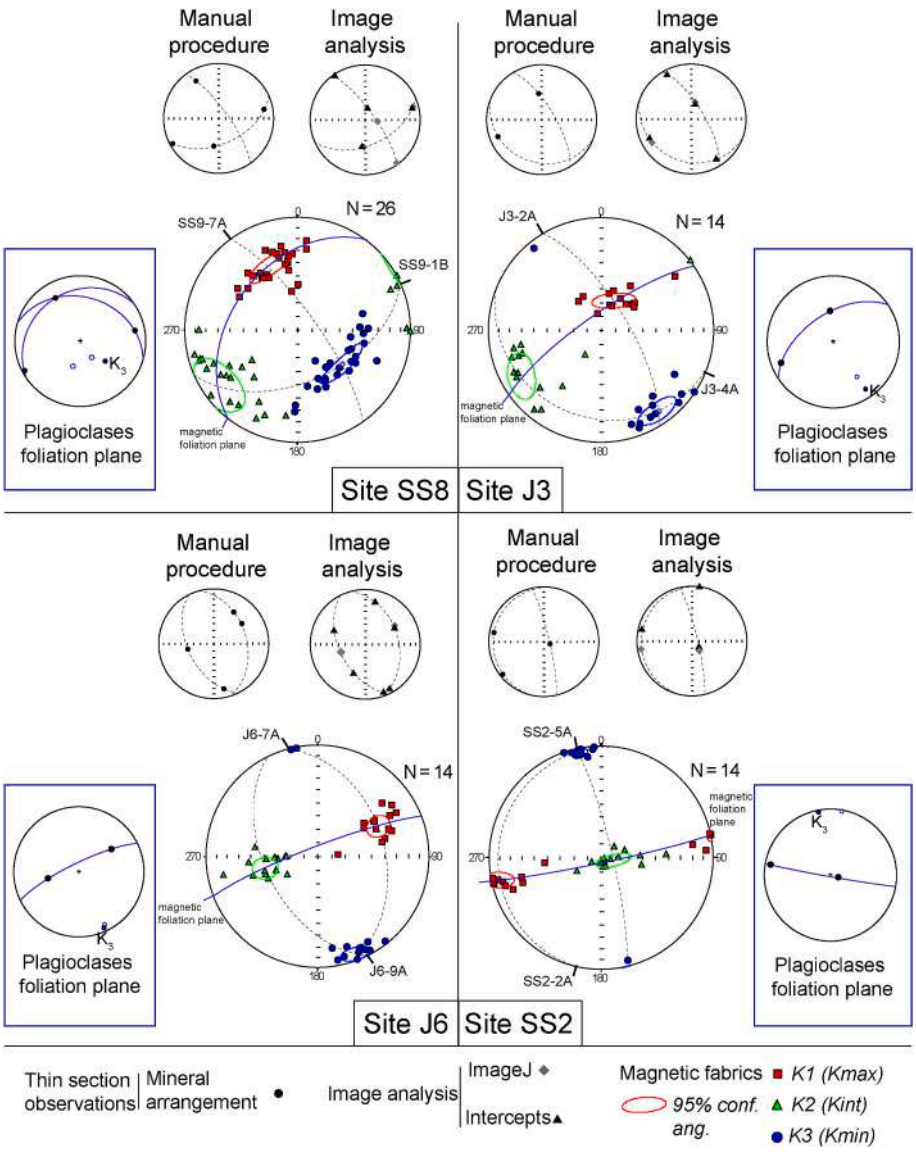

Fig. 11. Comparison between magnetic fabric results and microstructural observation. The foliation defined by the arrangement of the microlithic plagioclases is parallel or subparallel to the magnetic foliation plane (it is perpendicular to the K3 axis).

To conclude, the Sant Salvador intrusion is a special case with a magnetic fabric that clearly shows the flow direction, that is, parallel to the long axis of the preserved part of the intrusion. If we look at other examples in the literature, this relationship is not always so clear. These examples include magnetic lineation parallel to the magma flow of a single dike or a set of parallel dikes and the magnetic foliation broadly perpendicular to the subhorizontal layering, not representing the magma flow plane (Ferré et al., 2002). In the example described by Callot et al., (2001) the petrofabric of the plagioclases and the AMS results are also flow-related. They show a very good agreement between opaque preferred orientation and magnetic lineation, suggesting that the AMS signal is due either to a shape anisotropy of ferromagnetic grains mimicking the plagioclase, flow-related fabric or the alignment of grains. This fact is also observed by Diot et al., (2003) who observed magnetic subfabrics of the opaque minerals mimicking the primary petrofabric mainly defined by the shape-preferred orientation of the plagioclase and orthopyroxene crystals. In some of the above-cited examples, the oblate fabrics are flow-related when the foliation plane is close to parallel to the (walls of the) intrusive body, and also if this foliation is imbricated relative to side walls (Rochette et al., 1992; Callot and Geoffroy, 2004). This last feature is not observed in the Sant Salvador body, probably because the studied outcrops correspond to the inner part of the intrusion.

5.3. *The Sant Salvador body: geometry, orientation and emplacement*

The main challenge for interpreting the Sant Salvador intrusive body is that its geometry and orientation remain unknown due to its partial exposure in the field, where most of the body has been eroded, and also because of the lack of available data at depth. The orientation of the columnar jointing can be an indicator, never a determining factor, of the direction of magma flow and therefore, of the orientation of the intrusive body. Despite that, the magnetic fabric results, because of its close relationship with the petrofabric in this study, provide useful information that allows to constrain the spatial distribution of the intrusive body and to discard some previous hypotheses.

The pattern observed in magnetic fabrics is a magnetic lineation that progressively changes from a subvertical E-plunging attitude in the lower part of the intrusion, to a vertical arrangement in its middle part and finally to a subhorizontal orientation towards the uppermost part. In this case, the magnetic lineation (K_1 axes) represents the flow direction (Knight and Walker, 1988).

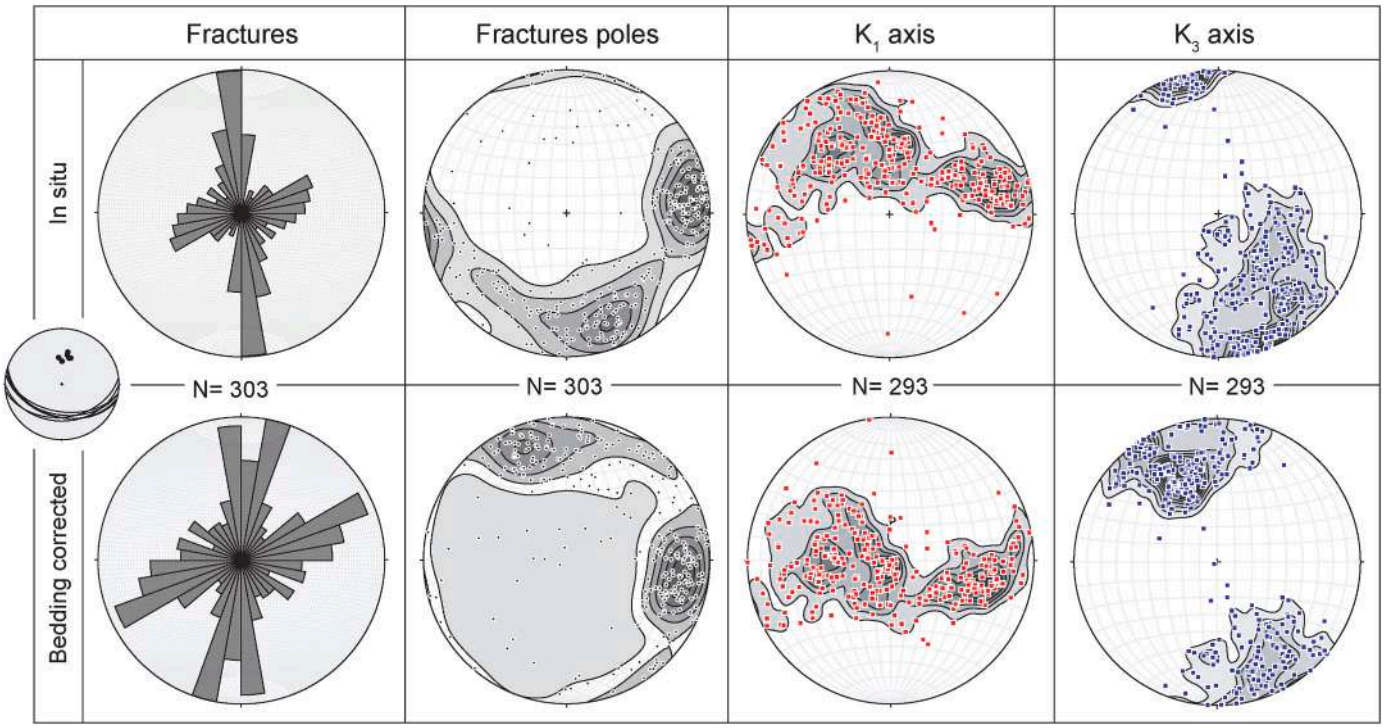

Fig. 12. Comparison between the fracture pattern of the intrusive body and the magnetic fabric results, before and after bedding restitution.

The magnetic fabric indicates the unidirectionality of the magma flow and the absence of multiple feeders. This is also supported by the constant orientation of the magnetic and mineral foliation, defined by the plagioclase, in the lower and middle part of the body. This is consistent with magma ascent along a vertical pipe as suggested by Gisbert (1981) where the flow forces dispose the tabular faces of the plagioclases parallel or subparallel to the magma flow direction. In its uppermost part, the change towards a subhorizontal direction indicates a change in the flow kinematics, spreading laterally at a certain depth close to the surface because of the change in pressure conditions. Horizontal K_1 orientations have been observed in other studies and are interpreted in dykes as local flow variations within a segment or at its tips (Wiegand et al., 2017) that may reflect a lateral propagation of one dyke segment towards an adjacent one.

At this point, the field information available and the exposure conditions do not allow to determine with certainty the geometry of the

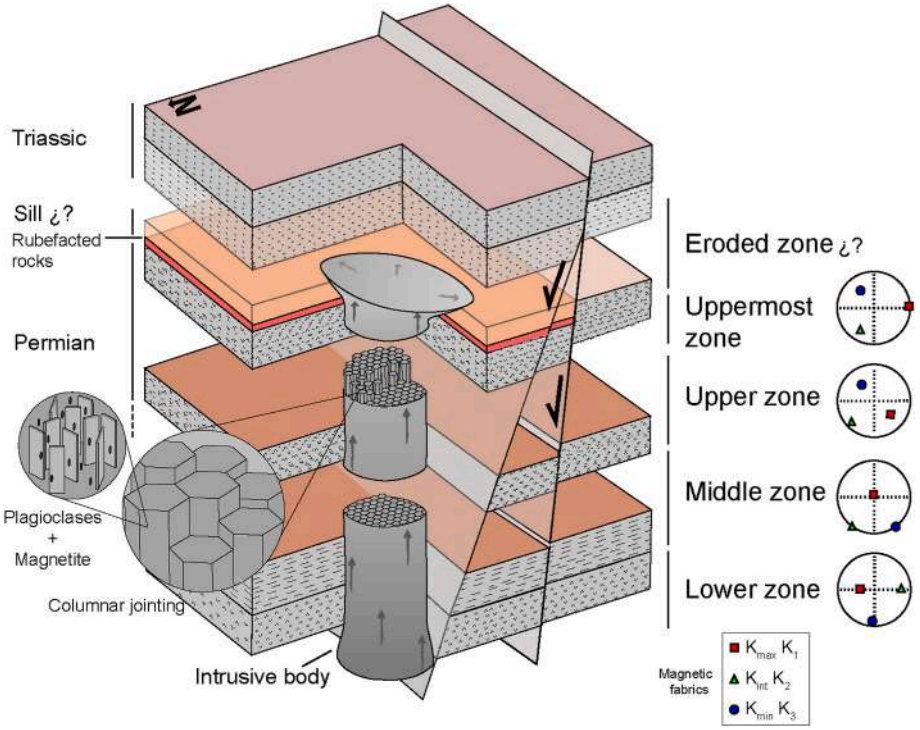

Fig. 13. Interpretation of stratigraphic sequence.

body from this level upwards. Nonetheless, the fact that there are not changes in its trachytic texture suggests that the magma remained at a certain depth below the surface. The constant orientation of the foliation and the structural data point towards Rochette et al. (1991, 1992) fabric type I. In this category, the averaged maximum and intermediate susceptibility axes lie within the dyke plane and the minimum axis is normal to the flow plane. Even the anomalous magnetic fabric of site J2 does not show a tendency different from the other magnetic fabric of the sampling profile.

According to the magnetic fabrics obtained, in its eroded upper part the body probably had a sill geometry (horizontal K_1 in the restored section). The poor exposure close to the contact of the intrusion of the reddish breccia and the reddish polygenetic microconglomerates and sandstones from the URU, do not allow to obtain conclusive data to characterize the deformation of the overlying beds due to the intrusion of the sill. Even so, the bedding data for the URU in this zone follow the regional trend of the red beds, which points to an erosional stage that could sweep away both the sill and a certain amount of materials of the URU overlying it (Fig. 13). The dimensions of the intrusive body are small regardless of its being a dike or a pipe. For these cases the magma flow is almost always laminar, it has defined direction for long distances and its cooling times are much shorter than in intrusive bodies of irregular form and large dimensions such as granites (Cañón-Tapia, 2004).

Interestingly, the flow direction in the uppermost part of the intrusion, in the knickpoint between vertical and horizontal feeding, is E-W, that is the dominant direction obtained for most of the volcanic products during the Stephanian main eruption stage (responsible for volcaniclastic deposits and lava flows) in the Cadí basin (Martí Molist and Mitjavila, 1988; Simón-Muzás et al., 2022). This means that flow in the upper part (hypothetical sill) of the Sant Salvador body followed the general trend of the topographic features, responding to faults with Pyrenean direction. In this sense, the main WNW-ESE structures limiting the Cadí basin and controlling sedimentation during the Late Carboniferous and the Permian exerted a control on the expansion and flow of magma, that spread parallel to these faults.

Regarding the tectonic context where the Sant Salvador intrusion was emplaced, several authors describe it (Gisbert, 1981; Bixel, 1984) as a subvertical, strike slip fault. It seems that the pre-existing structures influenced the orientation and the geometry of the Sant Salvador body. Besides, some authors consider sinistral displacements between different segments of the Sant Salvador intrusion caused by fractures striking N70 (Gisbert, 1981) or E-W faults (Bixel, 1984). However, the new data obtained in this study point to a very small (if existing) displacement on these fractures, that would be rather related to the columnar jointing of the intrusive body and not to a subsequent tectonic fracturing stage. The fact that the outcrop of the intrusion is restricted to the lower part of the stratigraphic sequence, the GU and the Palaeozoic basement, seems to be related to the E-W faults affecting these materials. Our interpretation (Fig. 1C) provides an explanation to this question: at present the intrusion only crops out in a restricted area due to the subsequent faulting and is probably cut at its base by the basal thrust of the Cadí thrust sheet.

6. Conclusions

Despite being a detailed study of a small intrusive body, the results of this work overpass the regional scale and have broader implications related with the faults at depth that allows the ascent of magma. This study is also exposed as an example of AMS in intrusive rocks and the relationships between columnar jointing and their internal fabric.

The conclusions obtained in this study can be summarized as follows:

- The main magnetic carriers of the AMS are ferrimagnetic minerals, magnetite/titanomagnetite whereas the contribution of plagioclase to the overall susceptibility is negligible. The high values of susceptibility respect to the rocks that surround the intrusion may be due to small-scale enrichment in ferromagnetic minerals during its emplacement. Preferred distribution of minerals along the feeding pipe is reflected in a density gradient, diminishing from bottom to top.
- AMS results reflect the primary fabric of the rock, originated during the emplacement of the intrusion.
- In all the studied samples the magnetic foliation is subparallel to the foliation plane defined by the preferred arrangement of the plagioclases observed under the optical microscope. This indicates that, despite the fact that plagioclase crystals do not contribute to the magnetic fabric, the ferromagnetic fabric mimics the petrofabric. The ferromagnetic minerals have been formed during the emplacement of the magma or due to a later process but in the interstices or exolved in the plagioclase and with the same orientation as the primary fabric.
- The magmatic foliation defined by plagioclases and the magnetic foliation are parallel to the ENE-WSW jointing family set. The foliation defined by the plagioclases is a plane of weakness that favored the formation of one of the joint sets.
- In an overall view, the magnetic fabrics corresponds with the features obtained from microstructural analysis. Manual procedures under the optical microscope represents for this case of study, the best tool to obtain the foliation plane instead of the automated image analysis.
- The Sant Salvador body intruded by a unidirectional magma flow through a vertical pipe that in the uppermost part spread over as a sill. An important erosion precluded the preservation of previous materials covering the upper part of the intrusion.

Authorship statement

Ana Simón-Muzás: Investigation, Formal analysis, Visualization, Writing - Original Draft. Antonio M. Casas-Sainz: Conceptualization, Investigation, Project administration, Supervision. Ruth Roto: Project administration, Investigation, Supervision. Josep Gisbert: Resources. Elisabet Beamud: Resources, Investigation.

Declaration of competing interest

The authors declare that they have no known competing financial interests or personal relationships that could have appeared to influence the work reported in this paper.

Acknowledgements

The authors are very grateful to Ana B. Arauzo from the Department of Physics, University of Zaragoza, for their help and explanations during the realization of the hysteresis cycles. Authors would like to acknowledge the use of Servicio General de Apoyo a la Investigación-SAI, Universidad de Zaragoza that carried out the thin sections of samples. This work was supported by projects grants PID2020-114273 GB-C22, PID2019-108753 GB-C22 and FPU19/02353 funded by MCIN/AEI/10.13039/501100011033, “ERDF Away of making Europe” and “ESF Investing in your future”. EB thanks the Geomodels Research Institute (UB) and GGAC 2021 SGR00076 (AGAUR). Also we are grateful to Bjarne Almqvist and an anonymous reviewer for their careful revision of the manuscript.

References

Almqvist, B.S., Bosshard, S.A., Hirt, A.M., Mattsson, H.B., Hetényi, G., 2012. Internal flow structures in columnar jointed basalt from Hrepphólar, Iceland: II. Magnetic anisotropy and rock magnetic properties. Bull. Volcanol. 74 (7), 1667–1681.

Aranguren, A., Cuevas, J., Tubia, J.M., Román-Berdiel, T., Casas-Sainz, A., Casas-Ponsati, A., 2003. Granite laccolith emplacement in the Iberian arc: AMS and gravity study of the La Tojiza pluton (NW Spain). J. Geol. Soc. 160 (3), 435–445.

Bascou, J., Camps, P., Dautria, J.M., 2005. Magnetic versus crystallographic fabrics in a basaltic lava flow. J. Volcanol. Geoth. Res. 145, 119–135.
Bixel, F., 1984. Le Volcanisme Stéphano-Permien des Pyrénées. Thèse d'Etat Université deToulouse, p. 639.
Borradaile, G.J., Henry, B., 1997. Tectonic applications of magnetic susceptibility and its anisotropy. Earth Sci. Rev. 42 (1–2), 49–93.
Bouchez, J.L., 1997. Granite is never isotropic: an introduction to AMS studies of granitic rocks. In: Granite: from Segregation of Melt to Emplacement Fabrics. Springer, Dordrecht, pp. 95–112.
Budkewitsch, P., Robin, P.Y., 1994. Modelling the evolution of columnar joints. J. Volcanol. Geoth. Res. 59 (3), 219–239.
Callot, J.P., Geoffroy, L., Aubourg, C., Pozzi, J.P., Mege, D., 2001. Magma flow directions of shallow dykes from the East Greenland volcanic margin inferred from magnetic fabric studies. Tectonophysics 335 (3–4), 313–329.
Callot, J.P., Geoffroy, L., 2004. Magma flow in the East Greenland dyke swarm inferred from study of anisotropy of magnetic susceptibility: magmatic growth of a volcanic margin. Geophys. J. Int. 159 (2), 816–830.
Cañón-Tapia, E., 2004. Anisotropy of magnetic susceptibility of lava flows and dykes: a historical account. Geol. Soc. Lond., Spec. Publ. 238 (1), 205–225.
Chadima, M., Jelínek, V., 2019. Anisoft5.1.03: Anisotropy Data Browser for Windows. Agico, Inc.
Chadima, M., Hrouda, F., 2012. Cureval 8.0: Thermomagnetic Curve Browser forWindows. Agico, Inc.
Cruden, A.R., McCaffrey, K.J., Bunger, A.P., 2017. Geometric scaling of tabular igneous intrusions: implications for emplacement and growth. In: Physical Geology of Shallow Magmatic Systems. Springer, Cham, pp. 11–38.
Diarte-Blasco, P., Casas, A.M., Pocoví, A., Villalaín, J.J., Muñoz, A., Beolchini, V., Pueyo-Anchuela, O., Peña-Chocarro, L., 2020. Interpretation of magnetic anomalies of geological and archaeological origins in a volcanic area (Tusculum site, Lazio, Italy): methodological proposals. J. Appl. Geophys. 173, 103942.
Diot, H., Bolle, O., Lambert, J.M., Launeau, P., Duchesne, J.C., 2003. The Tellnes ilmenite deposit (Rogaland, South Norway): magnetic and petrofabric evidence for emplacement of a Ti-enriched noritic crystal mush in a fracture zone. J. Struct. Geol. 25 (4), 481–501.
Feinberg, J.M., Wenk, H.R., Scott, G.R., Renne, P.R., 2006. Preferred orientation and anisotropy of seismic and magnetic properties in gabbronorites from the Bushveld layered intrusion. Tectonophysics 420 (3–4), 345–356.
Ferré, E.C., Bordarier, C., Marsh, J.S., 2002. Magma flow inferred from AMS fabrics in a layered mafic sill, Insizwa, South Africa. Tectonophysics 354 (1–2), 1–23.
Gisbert, J., 1981. Estudio Geológico - Petrológico del Estefaniense – Pérmico de la Sierra del Cadi (Pirineo de Lérida). Diagenesis y Sedimentología. Unpublished PhD. Universidad de Zaragoza, p. 472.
Gleizes, G., Leblanc, D., Santana, V., Olivier, P., Bouchez, J.L., 1998. Sigmoidal structures featuring dextral shear during emplacement of the Hercynian granite complex of Cauterets–Panticosa (Pyrenees). J. Struct. Geol. 20 (9–10), 1229–1245.
Gudmundsson, A., 2012. Magma chambers: formation, local stresses, excess pressures, and compartments. J. Volcanol. Geoth. Res. 237, 19–41.
Hargraves, R.B., Johnson, D., Chan, C.Y., 1991. Distribution anisotropy: the cause of AMS in igneous rocks? Geophys. Res. Lett. 18, 2193–2196.
Hetényi, G., Taisne, B., Garel, F., Médard, É., Bosshard, S., Mattsson, H.B., 2012. Scales of columnar jointing in igneous rocks: field measurements and controlling factors. Bull. Volcanol. 74 (2), 457–482.
Hetényi, G., Milazzo, M.P., 2014. Columnar joints. Encyclopedia of planetary landforms 1–7.
Horsman, E., Tikoff, B., Morgan, S., 2005. Emplacement-related fabric and multiple sheets in the Maiden Creek sill, Henry mountains, Utah, USA. J. Struct. Geol. 27 (8), 1426–1444.
Hoyer, L., 2015. Rock Fabric Study of Karoo Dolerite Sills along the KwaZulu-Natal North Coast, South Africa: Implications for the Magma source(Doctoral Dissertation).
Hutton, D.H., 1988. Igneous emplacement in a shear-zone termination: the biotite granite at Strontian, Scotland. Geol. Soc. Am. Bull. 100 (9), 1392–1399.
Jelinek, V., 1977. The statistical theory of measuring anisotropy of magnetic susceptibility of rocks and its application. Geofyzika Brno 89p.
Jelinek, V., 1981. Characterization of the magnetic fabric of rocks. Tectonophysics 79, 63–70.
Kligfield, R., Lowrie, W., Hirt, A., Siddans, A.W.B., 1983. Effect of progressive deformation on remanent magnetization of Permian redbeds from the Alpes Maritimes (France). Tectonophysics 98 (1–2), 59–85.
Knight, M.D., Walker, G.P., 1988. Magma flow directions in dikes of the Koolau Complex, Oahu, determined from magnetic fabric studies. J. Geophys. Res. Solid Earth 93 (B5), 4301–4319.
Lago, M., Arranz, E., Pocovi, A., Galé, C., Gil-Imaz, A., 2004. Permian magmatism and basin dynamics in the southern Pyrenees: a record of the transition from late Variscan transtension to early Alpine extension. Geological Society, London 223 (1), 439–464. Special Publications.
Lamur, A., Lavallée, Y., Iddon, F., et al., 2018. Disclosing the temperature of columnar jointing in lavas. Nat. Commun. 9, 1432. https://doi.org/10.1038/s41467-018-03842-4.
Launeau, P., Robin, P.Y., 1996. Fabric analysis using the intercept method. Tectonophysics 267, 91–119.
Leblanc, D., Gleizes, G., Roux, L., Bouchez, J.L., 1996. Variscan dextral transpression in the French Pyrenees: new data from the Pic des Trois-Seigneurs granodiorite and its country rocks. Tectonophysics 261 (4), 331–345.
Lowrie, W., 1990. Identification of ferromagnetic minerals in a rock by coercivity and unblocking temperature properties. Geophys. Res. Lett. 17, 159–162. https://doi.org/10.1029/GL017i002p00159.
Martí Molist, J., Mitjavila, J., 1988. El volcanisimo tardihercínico del Pirineo Catalán, II: caracterización de la actividad explosiva.
Mattsson, H.B., Caricchi, L., Almqvist, B.S., Caddick, M.J., Bosshard, S.A., Hetényi, G., Hirt, A.M., 2011. Melt migration in basalt columns driven by crystallization-induced pressure gradients. Nat. Commun. 2 (1), 299.
Menand, T., 2011. Physical controls and depth of emplacement of igneous bodies: a review. Tectonophysics 500 (1–4), 11–19.
Muñoz, J.A., 1992. Evolution of a Continental Collision Belt: ECORS-Pyrenees Crustal Balanced Cross-Section. Thrust Tectonics. Springer, Dordrecht, pp. 235–246.
Nédélec, A., Bouchez, J.L., 2015. Granites: Petrology, Structure, Geological Setting, and Metallogeny. OUP, Oxford.
Nye, J.F., 1957. The Physical Properties of Crystals: Their Representation by Tensors and Matrices. Clarendon Press, Oxford, p. 333.
Oliva-Urcia, B., Casas, A.M., Ramón, M.J., Leiss, B., Mariani, E., Román-Berdiel, T., 2012. On the reliability of AMS in ilmenite-type granites: an insight from the Marimanha pluton, Central Pyrenees. Geophys. J. Int. 189 (1), 187–203.
Ort, M.H., Newkirk, T.T., Vilas, J.F., Vazquez, J.A., 2015. Towards the definition of AMS facies in the deposits of pyroclastic density currents. Geol. Soc. Lond., Spec. Publ. 396 (1), 205–226.
Paterson, G.A., Zhao, X., Jackson, M., Heslop, D., 2018. Measuring, processing, and analyzing hysteresis data. G-cubed 19 (7), 1925–1945. https://doi.org/10.1029/2018GC007620.
Petraske, A.K., Hodge, D.S., Shaw, R., 1978. Mechanics of emplacement of basic intrusions. Tectonophysics 46 (1–2), 41–63.
Rivalta, E., Taisne, B., Bunger, A.P., Katz, R.F., 2015. A review of mechanical models of dike propagation: schools of thought, results and future directions. Tectonophysics 638, 1–42.
Rochette, P., Jenatton, L., Dupuy, C., Boudier, F., Reuber, I., 1991. Diabase dikes emplacement in the Oman ophiolite: a magnetic fabric study with reference to geochemistry. In: Peters, T., Nicolas, A., Coleman, R.G. (Eds.), Ophiolite Genesis and Evolution of the Oceanic Lithosphere, Petrology and Structural Geology. Springer Netherlands, Dordrecht. https://doi.org/10.1007/978-94-011-3358-6.
Rochette, P., Jackson, M., Aubourg, C., 1992. Rock magnetism and the interpretation of anisotropy of magnetic susceptibility. Rev. Geophys. 30, 209. https://doi.org/10.1029/92RG00733.
Román-Berdiel, T., Pueyo-Morer, E.L., Casas-Sainz, A.M., 1995. Granite emplacement during contemporary shortening and normal faulting: structural and magnetic study of the Veiga Massif (NW Spain). J. Struct. Geol. 17 (12), 1689–1706.
Sant'Ovaia, H., Olivier, P., Ferreira, N., Noronha, F., Leblanc, D., 2010. Magmatic structures and kinematics emplacement of the Variscan granites from Central Portugal (Serra da Estrela and Castro Daire areas). J. Struct. Geol. 32 (10), 1450–1465.
Saura, E., Teixell, A., 2006. Inversion of small basins: effects on structural variations at the leading edge of the Axial Zone antiformal stack (Southern Pyrenees, Spain). J. Struct. Geol. 28 (11), 1909–1920.
Schneider, C.A., Rasband, W.S., Eliceiri, K.W., 2012. NIH Image to ImageJ: 25 years of image analysis. Nat. Methods 9, 671–675.
Simón-Muzás, A., Casas-Sainz, A.M., Soto, R., Gisbert, J., Román-Berdiel, T., Oliva-Urcia, B., Pueyo, E.L., Beamud, E., 2022. Axial longitudinal flow in volcanic materials of the Late Carboniferous-Permian Cadí basin (Southern Pyrenees) determined from anisotropy of magnetic susceptibility. J. Volcanol. Geoth. Res. (421), 107443 https://doi.org/10.1016/j.jvolgeores.2021.107443.
Stacey, F.D., 1960. Magnetic anisotropy of igneous rocks. J. Geophys. Res. 65 (8), 2429–2442.
Tarling, D., Hrouda, F. (Eds.), 1993. Magnetic Anisotropy of Rocks. Chapman and Hall, London, p. 214.
Tauxe, L., 2008. Essentials of Paleomagnetism. 948. University of California Press.
Wiegand, M., Trumbull, R.B., Kontny, A., Greiling, R.O., 2017. An AMS study of magma transport and emplacement mechanisms in mafic dykes from the Etendeka Province, Namibia. Tectonophysics 716, 149–167.